The Journal of Chemical Physics

Nuclear polarization effects in cryptochrome-based magnetoreception

Cite as: J. Chem. Phys. **154**, 035102 (2021); https://doi.org/10.1063/5.0038947
Submitted: 28 November 2020 . Accepted: 22 December 2020 . Published Online: 15 January 2021

Siu Ying Wong, Ilia A. Solov'yov, P. J. Hore, and Daniel R. Kattnig

The Journal of Chemical Physics ARTICLE scitation.org/journal/jcp

Nuclear polarization effects in cryptochrome-based magnetoreception

Cite as: J. Chem. Phys. 154, 035102 (2021); doi: 10.1063/5.0038947
Submitted: 28 November 2020 • Accepted: 22 December 2020 •
Published Online: 15 January 2021

Siu Ying Wong,[1] Ilia A. Solov'yov,[1] P. J. Hore,[2,a)] and Daniel R. Kattnig[3]

AFFILIATIONS

[1]Institut für Physik, Carl-von-Ossietzky Universität Oldenburg, 26111 Oldenburg, Germany
[2]Department of Chemistry, University of Oxford, Oxford OX1 3QZ, United Kingdom
[3]Living Systems Institute and Department of Physics, University of Exeter, Exeter EX4 4QD, United Kingdom

[a)]**Author to whom correspondence should be addressed:** peter.hore@chem.ox.ac.uk

ABSTRACT

The mechanism of the magnetic compass sense of migratory songbirds is thought to involve magnetically sensitive chemical reactions of light-induced radical pairs in cryptochrome proteins located in the birds' eyes. However, it is not yet clear whether this mechanism would be sensitive enough to form the basis of a viable compass. In the present work, we report spin dynamics simulations of models of cryptochrome-based radical pairs to assess whether accumulation of nuclear spin polarization in multiple photocycles could lead to significant enhancements in the sensitivity with which the proteins respond to the direction of the geomagnetic field. Although buildup of nuclear polarization appears to offer sensitivity advantages in the more idealized model systems studied, we find that these enhancements do not carry over to conditions that more closely resemble the situation thought to exist *in vivo*. On the basis of these simulations, we conclude that buildup of nuclear polarization seems unlikely to be a source of significant improvements in the performance of cryptochrome-based radical pair magnetoreceptors.

I. INTRODUCTION

Night-migratory songbirds can sense the direction of the Earth's magnetic field as an aid to navigation.[1–5] The primary sensors, located in the eyes,[6–8] pass information to a specific part of the bird's visual system in the brain for processing and integration with other orientation cues.[9,10] The leading hypothesis for the mechanism of this remarkable ability is the radical pair mechanism (RPM)[11–14] involving photochemical reactions of proteins known as cryptochromes,[12,15,16] which have been found in various cell types in the birds' retinas.[17–21] Spin-selectivity in the decay pathways of light-induced radical pairs in these proteins is thought to allow the direction of the geomagnetic field to influence the yield of a signaling state, providing the basis for a chemical inclination compass.[13] Studies of the purified proteins indicate that cryptochromes may indeed be fit for purpose as magnetic compass sensors.[16,22,23]

We consider the reaction cycle in Fig. 1, which has been used extensively to discuss the magnetic sensitivity of cryptochromes studied *in vitro*.[13,16] Photo-excitation of the FAD (flavin adenine dinucleotide) chromophore in the protein's diamagnetic electronic ground state (GS; rate constant, k_{ex}) produces a radical pair, denoted RP1, via sequential electron transfers from a chain of three or four tryptophan (TrpH) residues to the FAD excited singlet state (see Fig. S5 of the supplementary material for a diagram of the FAD and the Trp-tetrad). RP1, which comprises $FAD^{\bullet-}$ and $TrpH^{\bullet+}$ radicals, can either revert to the ground state by back electron transfer (rate constant, k_S) or form a stabilized radical pair, RP2, in which the tryptophan radical ($Trp^{\bullet}$) has been deprotonated (rate constant, k_F). The former occurs exclusively from the singlet state of RP1, while the latter is not spin-dependent and occurs at the same rate for singlet and triplet pairs. We assume that RP2 leads to a signaling state of the protein (not shown in Fig. 1) that initiates magnetic signal transduction and that this process eventually returns the protein to its ground state (overall rate constant, k_R).

The RPM, originally proposed by Kaptein and Oosterhoff[24] and Closs[25] to explain the origin of nuclear spin polarization

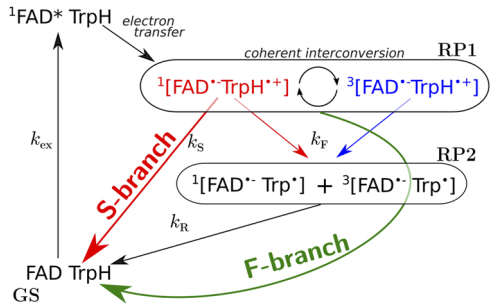

FIG. 1. Cryptochrome photocycle showing the formation and reaction pathways of the radical pairs RP1 and RP2. GS denotes the electronic ground state of the protein. The two routes by which the ground state is regenerated are referred to as the S- and F-branches, where S and F refer to singlet (recombination) and forward (reaction), respectively. ^{1}FAD* is the excited singlet state of the FAD chromophore. Superscripts 1 and 3 indicate singlet and triplet states, respectively.

arising in the reactions of organic radicals, is an attractive hypothesis for avian magnetoreception. It rationalizes the light-dependence of the magnetic compass sense,[26,27] is consistent with the observation that the compass is axial rather than polar,[2,3] and, at least qualitatively, can account for the effects of radiofrequency magnetic fields on the ability of caged songbirds to orient using the geomagnetic field.[28–30] One of the main factors that limits the detection sensitivity of this mechanism appears to be the spin-coherence lifetime of the magnetically sensitive radical pair,[31,32] which can be probed by behavioral experiments in which caged birds are exposed to radiofrequency magnetic fields superimposed on the Earth's field.[28,29,33–35] Given the crucial role in the mechanism played by nuclear spins via their hyperfine interactions and the fact that nuclear spins usually relax much less rapidly than electron spins, we wondered whether the magnetic detection sensitivity could be enhanced by the accumulation of nuclear spin polarization within the protein. Our use of the term "nuclear polarization" here refers to any non-equilibrium population of nuclear spin states whether in the radical pairs or in the ground state of the protein.

Singlet ↔ triplet interconversion is driven by hyperfine interactions in the radical pair and thus depends on the initial nuclear spin state.[24] Different nuclear spin states favor the formation of particular reaction products, a phenomenon commonly known as "spin-sorting."[24,36,37] By preserving the nuclear state populations over multiple photocycles, it may be possible to achieve an RP2 yield that deviates significantly from that in the first cycle. We are interested here in whether higher RP2 yield anisotropies [$\Delta\Phi_{RP2}$, defined in Eq. (20), Sec. II E] could be obtained when nuclear polarization is preserved in this way, possibly circumventing the limits to compass sensitivity imposed by (fast) electron spin relaxation.[31]

Nuclear polarization generated by intra-protein radical pairs has been observed by solid-state NMR (nuclear magnetic resonance) in mutant forms of the LOV (light-oxygen-voltage) domains of the flavoprotein phototropin,[38–40] but not, so far, in any cryptochrome.

II. THEORY

An important feature of the photocycle (Fig. 1) is that the ground state is regenerated by two routes: the "singlet branch," S (reverse electron transfer within the singlet state of RP1), and the "forward branch," F (formation and recycling of RP2). Depending on the timescales of these processes compared to the rates of nuclear spin relaxation and photoexcitation, it is possible that nuclear polarization generated in one photocycle can persist in the diamagnetic ground state and be carried forward to the following photocycle when the ground state is next excited. The likelihood that nuclear polarization survives is expected to be different for the two branches. The S-branch reaction has typical rate constants, k_S, between 10^5 s^{-1} and 10^7 s^{-1}, making it relatively fast.[16] Although k_F falls in the same range, overall, the F-branch is slower because it is rate-limited by the recycling of RP2. This process must allow adequate time for the geomagnetic field effect encoded in the yield of RP2 to be passed on in the initial stage of the signal transduction cascade.[13,41] Furthermore, nuclear spin relaxation is expected to be faster in the paramagnetic RP2 state than in the diamagnetic ground state, making it less likely that nuclear polarization would survive in the F-branch. We therefore consider three limiting cases: (1) full retention of nuclear polarization via both S- and F-branches, (2) preservation of nuclear polarization solely via the S-branch, and, for comparison, (3) the situation in which no nuclear polarization is passed from one cycle to the next. We do not consider here the possibility that nuclear polarizations could be enhanced by exploiting decoherence-free subspaces of the nuclear spin system.[42,43] This direction will be pursued in a future study.

A. Nuclear polarization mechanisms

The spin Hamiltonian of RP1 is written in angular frequency units as

$$\hat{H}_{RP1} = \boldsymbol{\omega}\cdot\hat{\mathbf{S}}_A + \boldsymbol{\omega}\cdot\hat{\mathbf{S}}_B + \sum_{i\in\{A,B\}}\sum_k \hat{\mathbf{S}}_i\cdot\mathbf{A}_{ik}\cdot\hat{\mathbf{I}}_{ik} + \hat{\mathbf{S}}_A\cdot\mathbf{D}\cdot\hat{\mathbf{S}}_B - J\left(2\hat{\mathbf{S}}_A\cdot\hat{\mathbf{S}}_B + \tfrac{1}{2}\right), \quad (1)$$

where $\hat{\mathbf{S}}_A$ and $\hat{\mathbf{S}}_B$ are the electron spin operators of the two radicals. $\boldsymbol{\omega} = -\gamma_e B(\sin\theta\cos\phi,\ \sin\theta\sin\phi,\ \cos\theta)$ is the geomagnetic field vector with magnitude $|\gamma_e|B$ (expressed as an angular frequency) and direction specified by the angles θ and ϕ. $\mathbf{A}_{ik}$ is the hyperfine tensor that couples nucleus k (spin operator $\hat{\mathbf{I}}_{ik}$) with the electron in radical i. $\mathbf{D}$ and J are the dipolar coupling tensor and the exchange interaction of the two electron spins, respectively. We also define the dipolar coupling parameter D such that the eigenvalues of $\mathbf{D}$ are $\{4D/3, -2D/3, -2D/3\}$. Values of $\mathbf{A}_{ik}$, $\mathbf{D}$, D, and J are quoted in MHz in the following text; they can be converted to angular frequencies by multiplying by 2π.

Since $\hat{H}_{RP1}$ acts on both the electronic and nuclear parts of the density operator, $\hat{\rho}_{RP1}(t)$, evolution of $\hat{\rho}_{RP1}(t)$ under $\hat{H}_{RP1}$ allows generation of nuclear polarization in the proposed photocycle via three mechanisms, originally identified in the context of photo-CIDNP (chemically induced dynamic nuclear polarization) observed by solid-state NMR of photosynthetic reaction centers:[44,45] differential relaxation (DR),[46,47] differential decay (DD),[48] and three-spin mixing (TSM).[49,50]

First, polarization can arise as a consequence of the aforementioned spin-sorting process if the reaction products have different nuclear spin relaxation rates. This is precisely the scenario described above in which polarization is lost in the slower F-branch. If only S-branch nuclear polarizations are retained, the populations of nuclear states that disfavour singlet ↔ triplet interconversion would grow over multiple cycles at the expense of the populations of other states. This mechanism is commonly termed differential relaxation.[46,47] It makes no contribution when there is full retention of polarization in both branches. Second, nuclear polarization can also arise from a differential decay[48] mechanism, which relies on different rates of removal of singlet and triplet radical pairs and the presence of pseudosecular terms in the hyperfine coupling.[45] It is operative for our reaction scheme because the singlet state always reacts faster than the triplet (unless $k_S \ll k_F$, the case in which all magnetic field effects would be very small anyway). Finally, contributions to the nuclear polarization can be expected from a three-spin mixing[49,50] mechanism in which the dipolar coupling of the two electron spins causes spin-coherences arising from hyperfine interactions to evolve at different frequencies.[51] Assuming that the magnetic sensitivity arises principally in the form of RP1 that contains the third tryptophan of the "Trp-tetrad,"[52,53] the magnitude of the dipolar coupling is between 10 MHz and 15 MHz (see Sec. III A). As this is comparable to or larger than the hyperfine couplings in $FAD^{\bullet-}$ and $TrpH^{\bullet+}$ and the Zeeman interaction with the geomagnetic field (~50 μT or 1.4 MHz), we can anticipate a non-zero TSM contribution. The double-matching condition for the optimum nuclear polarization of a nucleus with isotropic hyperfine coupling a_{iso} and zero exchange coupling is given by $|\omega| \approx |D|3 \approx 4|a_{iso}|$ (Ref. 51). Note that, while often neglected in theoretical studies of cryptochromes' magnetosensitivity, electron–electron interactions have a strongly attenuating effect on the compass sensitivity.[54]

B. Nuclear polarization preserved in both branches

We start with the situation in which no nuclear polarization is lost in either branch of the photocycle and include the possibility that polarization generated in one branch may partially cancel that arising from the other. The equations of motion for the density operators of the three states of the protein, RP1, RP2, and GS, can be written as follows:

$$\frac{\mathrm{d}\hat{\rho}_{\mathrm{RP1}}(t)}{\mathrm{d}t} = k_{\mathrm{ex}}|\mathrm{S}\rangle\langle\mathrm{S}| \otimes \left(\hat{Q}\,\hat{\rho}_{\mathrm{GS}}(t)\right) - i\left[\hat{H}_{\mathrm{RP1}}, \hat{\rho}_{\mathrm{RP1}}(t)\right]_- - \frac{k_S}{2}\left[\hat{P}_S, \hat{\rho}_{\mathrm{RP1}}(t)\right]_+ - k_F\hat{\rho}_{\mathrm{RP1}}(t), \tag{2}$$

$$\frac{\mathrm{d}\hat{\rho}_{\mathrm{RP2}}(t)}{\mathrm{d}t} = -i\left[\hat{H}_{\mathrm{RP2}}, \hat{\rho}_{\mathrm{RP2}}(t)\right]_- + k_F\hat{\rho}_{\mathrm{RP1}}(t) - k_R\hat{\rho}_{\mathrm{RP2}}(t), \tag{3}$$

$$\frac{\mathrm{d}\hat{\rho}_{\mathrm{GS}}(t)}{\mathrm{d}t} = -k_{\mathrm{ex}}\hat{\rho}_{\mathrm{GS}}(t) + \frac{k_S}{2}\mathrm{Tr_e}\left[\left[\hat{P}_S, \hat{\rho}_{\mathrm{RP1}}(t)\right]_+\right] + k_R\mathrm{Tr_e}\left[\hat{\rho}_{\mathrm{RP2}}(t)\right]. \tag{4}$$

The corresponding Hilbert spaces have dimensions $4Z$, $4Z$, and Z, respectively, where Z is the total nuclear spin degeneracy,

$$Z = \prod_{i\in\{\mathrm{A,B}\}}\prod_k (2I_{ik}+1), \tag{5}$$

and I_{ik} is the spin quantum number of nucleus k in radical i.

In Eqs. (2)–(4), $\hat{H}_{\mathrm{RP1}}$ and $\hat{H}_{\mathrm{RP2}}$ are the radical pair spin Hamiltonians, $\hat{P}_S = |\mathrm{S}\rangle\langle\mathrm{S}| \otimes \hat{E}$ is the singlet projection operator, $\hat{E}$ is the identity operator in the nuclear-spin space, $[\hat{A}, \hat{B}]_\pm = \hat{A}\hat{B} \pm \hat{B}\hat{A}$, and $\mathrm{Tr_e}[\ldots]$ is the trace over the electron-spin space. A Haberkorn-type operator is used for the spin-selective reaction of the singlet state of RP1.[55]

We assume that the spin Hamiltonian of the diamagnetic ground state is dominated by the nuclear Zeeman interaction. We hence take the nuclear spins to be quantized in the Zeeman basis in which the eigenstates correspond to product basis states, specified by the magnetic quantum numbers $m_{i,k}$ of each nucleus in the spin system. $|j\rangle$ is used to denote these eigenstates, $|m_{\mathrm{A},1}, m_{\mathrm{A},2}\ldots\rangle$.

Transformation from the molecular basis (in which the calculation is performed) to the Zeeman basis can be achieved using the rotation operator $\hat{R}$,

$$\hat{R} = \exp\left(-i\hat{F}_z\phi\right)\exp\left(-i\hat{F}_y\theta\right), \tag{6}$$

where $\hat{F}_y$ and $\hat{F}_z$ are components of the total nuclear spin operator $\hat{\mathbf{F}}$, defined as

$$\hat{\mathbf{F}} = \sum_{i\in\{\mathrm{A,B}\}}\sum_k \hat{\mathbf{I}}_{ik}, \tag{7}$$

where $\hat{\mathbf{I}}_{ik}$ is the spin operator of nucleus k in radical i.

We also assume that all coherences in this basis dephase before the ground state is re-excited. Thus, only the Zeeman eigenstate populations are retained and passed on to RP1. This filtering is achieved by means of the superoperator $\hat{\hat{Q}}$ in Eq. (2), defined as

$$\hat{\hat{Q}}\,\hat{\tau} = \hat{R}\left(\sum_j^Z |j\rangle\langle j|\left(\hat{R}^\dagger\hat{\tau}\,\hat{R}\right)|j\rangle\langle j|\right)\hat{R}^\dagger. \tag{8}$$

$\hat{H}_{\mathrm{RP1}}$ is given by Eq. (1). For a more complete description of the F-branch, we also include the spin dynamics of RP2 by means of the spin Hamiltonian $\hat{H}_{\mathrm{RP2}}$, which is assumed to be identical to $\hat{H}_{\mathrm{RP1}}$ apart from the absence of the hyperfine interaction of the tryptophan indole proton in $\hat{H}_{\mathrm{RP2}}$ (where applicable).

Equations (2)–(4) were solved numerically under steady state (SS) conditions ($\mathrm{d}\hat{\rho}_i(t)/\mathrm{d}t = 0$) with the initial conditions

$$\hat{\rho}_{\mathrm{GS}}(0) = \frac{\hat{E}}{Z} \quad \text{and} \quad \hat{\rho}_{\mathrm{RP1}}(0) = \hat{\rho}_{\mathrm{RP2}}(0) = \hat{0}. \tag{9}$$

We note, however, that, for the irreducible spin Hamiltonians considered here, this steady-state is uniquely defined independent of the initial condition. Details of the calculation can be found in Sec. S1 of

the supplementary material. The fractions of the protein present as the GS, RP1, and RP2 were calculated using

$$c_{\mathrm{GS}}^{\mathrm{SS}} = \mathrm{Tr_n}\left[\hat{\rho}_{\mathrm{GS}}^{\mathrm{SS}}\right], \tag{10}$$

$$c_{\mathrm{RP1}}^{\mathrm{SS}} = \mathrm{Tr_{e,n}}\left[\hat{\rho}_{\mathrm{RP1}}^{\mathrm{SS}}\right], \tag{11}$$

$$c_{\mathrm{RP2}}^{\mathrm{SS}} = \mathrm{Tr_{e,n}}\left[\hat{\rho}_{\mathrm{RP2}}^{\mathrm{SS}}\right], \tag{12}$$

respectively, where $\mathrm{Tr_n}[\ldots]$ is the trace over the nuclear-spin space and $\mathrm{Tr_{e,n}}[\ldots]$ is the trace over the combined electron-nuclear Hilbert space. These three quantities sum to 1. However, for typical parameters, the lifespan of RP1 is short and its steady state fraction is very small. In this case,

$$c_{\mathrm{GS}}^{\mathrm{SS}} + c_{\mathrm{RP2}}^{\mathrm{SS}} \approx 1. \tag{13}$$

C. Nuclear polarization preserved in the S-branch

In the case that nuclear polarization is retained only in the S-branch, $\mathrm{d}\hat{\rho}_{\mathrm{RP1}}(t)/\mathrm{d}t$ is still given by Eq. (2), but Eqs. (3) and (4) are replaced by

$$\frac{\mathrm{d}c_{\mathrm{RP2}}(t)}{\mathrm{d}t} = k_{\mathrm{F}}\mathrm{Tr_{e,n}}\left[\hat{\rho}_{\mathrm{RP1}}(t)\right] - k_{\mathrm{R}}c_{\mathrm{RP2}}(t), \tag{14}$$

$$\frac{\mathrm{d}\hat{\rho}_{\mathrm{GS}}(t)}{\mathrm{d}t} = -k_{\mathrm{ex}}\hat{\rho}_{\mathrm{GS}}(t) + \frac{k_{\mathrm{S}}}{2}\,\mathrm{Tr_e}\left[\left[\hat{P}_{\mathrm{S}}, \hat{\rho}_{\mathrm{RP1}}(t)\right]_+\right] + k_{\mathrm{R}}c_{\mathrm{RP2}}(t)\frac{\hat{E}}{Z}, \tag{15}$$

where $c_{\mathrm{RP2}}(t) = \mathrm{Tr_{e,n}}\left[\hat{\rho}_{\mathrm{RP2}}(t)\right]$.

D. No preservation of nuclear polarization

Finally, when no nuclear polarization is transferred from one cycle to the next, Eqs. (2) and (4) are replaced by

$$\frac{\mathrm{d}\hat{\rho}_{\mathrm{RP1}}(t)}{\mathrm{d}t} = k_{\mathrm{ex}}c_{\mathrm{GS}}(t)|\mathrm{S}\rangle\langle\mathrm{S}| \otimes \frac{\hat{E}}{Z} - i\left[\hat{H}_{\mathrm{RP1}}, \hat{\rho}_{\mathrm{RP1}}(t)\right]_- - \frac{k_{\mathrm{S}}}{2}\left[\hat{P}_{\mathrm{S}}, \hat{\rho}_{\mathrm{RP1}}(t)\right]_+ - k_{\mathrm{F}}\hat{\rho}_{\mathrm{RP1}}(t), \tag{16}$$

$$\frac{\mathrm{d}c_{\mathrm{GS}}(t)}{\mathrm{d}t} = -k_{\mathrm{ex}}c_{\mathrm{GS}}(t) + \frac{k_{\mathrm{S}}}{2}\mathrm{Tr_{e,n}}\left[\left[\hat{P}_{\mathrm{S}}, \hat{\rho}_{\mathrm{RP1}}(t)\right]_+\right] + k_{\mathrm{R}}c_{\mathrm{RP2}}(t), \tag{17}$$

where $c_{\mathrm{GS}}(t) = \mathrm{Tr_n}\left[\hat{\rho}_{\mathrm{GS}}(t)\right]$ and $\mathrm{d}c_{\mathrm{RP2}}(t)/\mathrm{d}t$ is still given by Eq. (14).

E. Yield of signaling state

One way of quantifying the effects of recycling of nuclear polarization is to look at the variation in $c_{\mathrm{RP2}}^{\mathrm{SS}}$ with the direction of the geomagnetic field. However, $c_{\mathrm{RP2}}^{\mathrm{SS}}$ depends on the values of k_{R} and k_{ex}, neither of which is known *in vivo*. k_{R} depends on the signaling and recycling mechanism (about which very little is known[41]), and k_{ex} varies with the intensity and polarization of the light entering the bird's eye and the (unknown) number of magnetoreceptor molecules in the retina.[56,57] As a measure of the directional signal afforded by the radical pair, we therefore use Φ_{RP2}, the probability that RP1 reacts to form RP2, i.e., the quantum yield of the formation of the signaling state under steady state conditions. This quantity is calculated as

$$\Phi_{\mathrm{RP2}} = \frac{k_{\mathrm{F}}}{k_{\mathrm{F}} + k_{\mathrm{rec}}} = \frac{k_{\mathrm{R}}c_{\mathrm{RP2}}^{\mathrm{SS}}}{k_{\mathrm{ex}}c_{\mathrm{GS}}^{\mathrm{SS}}}, \tag{18}$$

where the k_{rec} is the recombination rate constant of RP1 in the steady state, defined by

$$k_{\mathrm{rec}}c_{\mathrm{RP1}}^{\mathrm{SS}} = \frac{k_{\mathrm{S}}}{2}\mathrm{Tr_{e,n}}\left[\left[\hat{P}_{\mathrm{S}}, \hat{\rho}_{\mathrm{RP1}}^{\mathrm{SS}}\right]_+\right]. \tag{19}$$

This relation is obtained by taking the trace of Eqs. (2)–(4), or the equivalent equations for the other scenarios, and making use of the normalization requirement $c_{\mathrm{GS}}^{\mathrm{SS}} + c_{\mathrm{RP1}}^{\mathrm{SS}} + c_{\mathrm{RP2}}^{\mathrm{SS}} = 1$. Φ_{RP2} is independent of k_{R} and k_{ex}, which makes it the measure of choice to analyze the effects of accumulated nuclear polarization.

Since RP2 goes on to form exclusively the signaling state, Φ_{RP2} is a convenient measure of the signaling efficiency and allows direct comparison with the calculations described in Sec. II F.

The sensitivity of the radical pair compass is then given by the extent to which Φ_{RP2} varies with the direction of the geomagnetic field,

$$\Delta\Phi_{\mathrm{RP2}} = \max_{\theta,\,\phi}(\Phi_{\mathrm{RP2}}) - \min_{\theta,\,\phi}(\Phi_{\mathrm{RP2}}), \tag{20}$$

where the maximum and minimum values of Φ_{RP2} are determined by sampling a large number of geomagnetic field directions, (θ, ϕ).

F. Sequential photocycles

To see how nuclear polarization builds up, we calculated the fractional yield of RP2 in sequential cycles around the reaction scheme in Fig. 1. For the nth cycle, when polarization is preserved in the S-branch only, this was done by integrating

$$\frac{\mathrm{d}\hat{\rho}_{\mathrm{RP1},n}(t)}{\mathrm{d}t} = -i\left[\hat{H}_{\mathrm{RP1}}, \hat{\rho}_{\mathrm{RP1},n}(t)\right]_- - \frac{k_{\mathrm{S}}}{2}\left[\hat{P}_{\mathrm{S}}, \hat{\rho}_{\mathrm{RP1},n}(t)\right]_+ - k_{\mathrm{F}}\hat{\rho}_{\mathrm{RP1},n}(t). \tag{21}$$

The initial condition for the first cycle ($n = 0$) is

$$\hat{\rho}_{\mathrm{RP1},0}(0) = |\mathrm{S}\rangle\langle\mathrm{S}| \otimes \frac{\hat{E}}{Z}, \tag{22}$$

while the initial condition for subsequent cycles is given by

$$\hat{\rho}_{\mathrm{RP1},n+1}(0) = |\mathrm{S}\rangle\langle\mathrm{S}| \otimes \left(\hat{\mathrm{Q}}\hat{\rho}_{\mathrm{GS},n}\right), \tag{23}$$

where $\hat{\rho}_{\mathrm{GS},n}$ is the ground state nuclear spin density operator at the end of cycle n,

$$\hat{\rho}_{\mathrm{GS},n} = \frac{k_{\mathrm{S}}}{2}\int_0^\infty \mathrm{Tr_e}\left[\left[\hat{P}_{\mathrm{S}}, \hat{\rho}_{\mathrm{RP1},n}(t)\right]_+\right]\mathrm{d}t + \frac{\hat{E}}{Z}k_{\mathrm{F}}\int_0^\infty \mathrm{Tr_{e,n}}\left[\hat{\rho}_{\mathrm{RP1},n}(t)\right]\mathrm{d}t. \tag{24}$$

The fraction of the protein generated as RP2 in cycle n is given by

$$\Phi_{\mathrm{RP2},n} = k_{\mathrm{F}}\int_0^\infty \mathrm{Tr_{e,n}}\left[\hat{\rho}_{\mathrm{RP1},n}(t)\right]\mathrm{d}t. \tag{25}$$

As n increases, $\Phi_{\mathrm{RP2},n}$ approaches the corresponding steady state value of Φ_{RP2} obtained using Eq. (18). When no nuclear polarization is passed from one cycle to the next, the initial state at the beginning of a cycle is always given by Eq. (22) and $\Phi_{\mathrm{RP2},n} = \Phi_{\mathrm{RP2},0}$ throughout. The corresponding steady state value of Φ_{RP2} when no polarization is retained, hereafter denoted $\Phi_{\mathrm{RP2}}^{\mathrm{nr}}$, is also equal to $\Phi_{\mathrm{RP2},0}$.

III. RESULTS AND DISCUSSION

A. Simulation parameters

To explore the effects of recycling nuclear polarization, we performed simulations for a variety of models of the [$\mathrm{FAD}^{\bullet-}$ $\mathrm{TrpH}^{\bullet+}$] radical pair. The required computational power scales steeply with the number of spins, making it impossible to include a full set of hyperfine interactions in $\mathrm{FAD}^{\bullet-}$ and $\mathrm{TrpH}^{\bullet+}$. We have therefore chosen to construct model radical pairs containing only the nuclei with the largest anisotropic hyperfine interactions in each radical (calculated using density functional theory; see Table S2 of the supplementary material) in the expectation that such calculations would provide a reasonable guide to the behavior of the complete system.[58] Specifically, hyperfine interactions were included for nuclei selected from the following set: in $\mathrm{FAD}^{\bullet-}$, the nitrogens N5 and N10 in the central ring of the isoalloxazine group and in $\mathrm{TrpH}^{\bullet+}$, the indole nitrogen, NE1, and its directly bonded proton, HE1 (see Fig. S4 of the supplementary material for the labeling scheme).

To model the configuration of $\mathrm{FAD}^{\bullet-}$ and $\mathrm{Trp_CH}^{\bullet+}$ (the third tryptophan of the tetrad) in avian cryptochrome, we considered the x-ray crystal structure of pigeon cryptochrome 4 (*Cl*Cry4).[59] The structure was used to obtain the dipolar tensor **D** [Eq. (1)], taking its axis as the vector connecting the centers of $\mathrm{FAD}^{\bullet-}$ and $\mathrm{Trp_CH}^{\bullet+}$. The length of the vector is 1.76 nm, corresponding to a dipolar coupling parameter D of −14.3 MHz. Its direction is given by ($\theta_{\mathrm{D}} = 0.40\pi$, $\phi_{\mathrm{D}} = 1.70\pi$) in the flavin axis system. The relative orientations of FAD and $\mathrm{Trp_CH}$ were also extracted to give hyperfine coupling tensors for the nuclei in $\mathrm{Trp_CH}^{\bullet+}$ (see Tables S2 and S3 and Fig. S6 of the supplementary material). As a comparison, we performed the same calculation on the averaged radical positions obtained from a molecular dynamics (MD) trajectory of a homology model of robin cryptochrome 4a (*Er*Cry4a) modeled from the *Cl*Cry4 crystal structure (see Sec. S5 of the supplementary material). The length of this vector is 1.82 nm, with $D = -13.0$ MHz, $\theta_{\mathrm{D}} = 0.34\pi$, and $\phi_{\mathrm{D}} = 1.68\pi$. Calculations using the relevant coupling tensors are hereafter referred to as using the *Cl*Cry4 or *Er*Cry4a MD configurations, respectively. In addition, in some of the simulations, we considered the dipolar coupling strength for [$\mathrm{FAD}^{\bullet-}$ $\mathrm{Trp_CH}^{\bullet+}$] obtained from electron paramagnetic resonance (EPR) measurements of purified *Er*Cry4a, which was −11.2 MHz.[60]

Spin dynamics calculations were performed using a molecular axis system in which the x-, y-, and z-axes were aligned with the short in-plane axis, the long in-plane axis, and the normal of the tricyclic ring system of the flavin radical, respectively (see Fig. S4 of the supplementary material). When present, the geomagnetic field was 50 μT with an orientation in this axis system defined by colatitude, θ, and azimuth, ϕ [Eq. (1)]. The default values of the rate constants were $k_{\mathrm{S}} = k_{\mathrm{F}} = 10^6\ \mathrm{s}^{-1}$. This choice ensures that the radical pair lives long enough (~1 μs) for a 50 μT field to affect Φ_{RP2}, but not so long that spin relaxation (not included in these calculations) would greatly attenuate the effects (see Sec. III E and Sec. S4 of the supplementary material) for simulations with different rate constants).

B. Dependence of Φ_{RP2} on the initial nuclear spin state

To get an initial impression of how sensitive the system is to nuclear polarization, we calculated Φ_{RP2} for a single pass through the photocycle using Eqs. (21)–(25) but with the initial condition [Eq. (22)] replaced by a density operator in which only one of the Z eigenstates of the ground state spin Hamiltonian was populated,

$$\hat{\rho}_{\mathrm{RP1}}(0) = |\mathrm{S}\rangle\langle\mathrm{S}| \otimes \left(\hat{R}\,|j\rangle\langle j|\hat{R}^{\dagger}\right). \tag{26}$$

The use of these extreme and highly artificial forms of $\hat{\rho}_{\mathrm{RP1}}(0)$ is intended to reveal the full range of possible nuclear polarization effects. Figure 2(a) shows the results for different subsets of nuclear spins with no electron dipolar or Zeeman interactions and with the two radicals aligned with their aromatic rings in the same plane. The nuclear spins in the ground state were assumed to be quantized along the flavin z-axis. The effect of the initial nuclear spin state is clear: for all subsets of nuclei apart from {N5, HE1} and {N5, N10, HE1}, there is a substantial spread in the yields of RP2, consistent with the nuclear spin-dependence of singlet-triplet interconversion. There is a clear difference between the average values of Φ_{RP2} (given at the top of the columns) with and without HE1 [right- and left-hand sides of Fig. 2(a), respectively]. With HE1 included, Φ_{RP2} is in the range 0.76–0.80; without HE1, it is in the range 0.61–0.67. We believe that this difference is connected to Kramers theorem and time-reversal symmetry[61,62] (see Sec. S3 of the supplementary material).

Figure 2(b) shows the outcome of the same calculation but now with the 50 μT geomagnetic field, applied parallel to the flavin z-axis ($\theta = 0$), and the *Cl*Cry4 configuration.

Once again, there is a broad range of Φ_{RP2} values for most of the model radical pairs. The higher average values of Φ_{RP2} here compared to Fig. 2(a) arise from the "low field effect" in which a

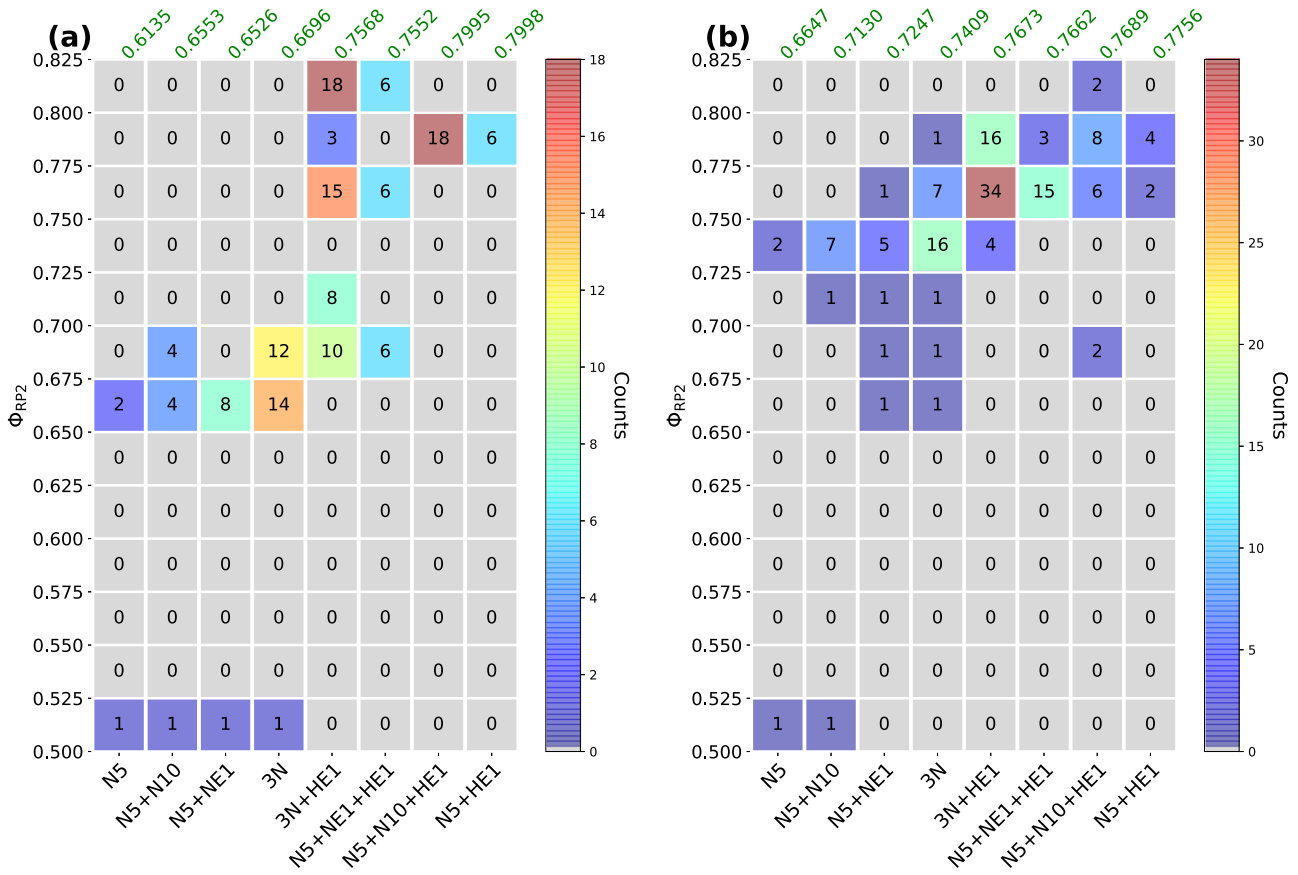

FIG. 2. Histograms of Φ_{RP2} values calculated for different subsets of the nuclear spins in [$FAD^{\bullet-}$ $TrpH^{\bullet+}$] with 100% initial occupation of each of the *Z* nuclear spin states, in turn, for each model radical pair. The label "3N" refers to the combination "N5 + N10 + NE1." The range of Φ_{RP2} values is divided into bins of width 0.025. The figures in the colored boxes give the number of initial nuclear spin states that yield a value of Φ_{RP2} within each bin. Within each column, these numbers sum to *Z*. The mean value of Φ_{RP2} for each spin system is given in green at the top of the column. (a) Without dipolar and Zeeman interactions; the flavin and indole rings were oriented in the same plane. (b) Dipolar and Zeeman interactions included; the *Cl*Cry4 configuration was used. In the bottom row of both panels, where Φ_{RP2} is in the range 0.500–0.525, the nitrogens are all initially in the $m = 0$ spin configuration.

weak applied magnetic field opens up new routes to the coherent conversion of singlet to triplet.[63,64]

C. One-nitrogen radical pair

The effects of retaining nuclear polarization are demonstrated in Fig. 3 for a model radical pair subject to the geomagnetic field. In this case, one of the electrons is coupled to a nitrogen nucleus with a hyperfine interaction that closely resembles that of N5 in $FAD^{\bullet-}$: the N5 hyperfine tensor was diagonalized, and the two smaller principal values were replaced by their average so that the interaction becomes axially symmetric (see Table S2 of the supplementary material). The dipolar coupling parameter *D* was the EPR value of −11.2 MHz for [$FAD^{\bullet-}$ $Trp_CH^{\bullet+}$] in *Er*Cry4a,[60] and the dipolar axis was parallel to the hyperfine axis. The other radical had no hyperfine interactions.

In Fig. 3(a), the geomagnetic field is parallel to the hyperfine axis ($\theta = 0$). The populations of each of the three N5 spin states at the beginning consecutive photocycles were calculated assuming retention of nuclear polarization in the S-branch only using Eqs. (21)–(25) with the results shown in dashed lines. Also shown are the corresponding steady state nuclear populations obtained using Eqs. (2), (14), and (15). The differences in the populations of the nuclear states accumulate with the number of photocycles, leveling off to the steady-state values after ~10 cycles.

The calculation of steady state nuclear populations was extended by varying θ, the angle between the geomagnetic field and the hyperfine axis. The results are given in Fig. 3(b). As expected from the anisotropy of the hyperfine interaction, the nuclear state populations depend on the field direction, with the greatest deviation from the equilibrium population (gray line) occurring when the field is aligned with the hyperfine axis ($\theta = 0, \pi$).

This anisotropy is reflected in the corresponding values of Φ_{RP2}. Figure 3(c) shows the steady-state values for the same range of θ, together with the values corresponding to no retention (equivalent to those at the end of the first photocycle, $\Phi_{RP2,n=1}$). Retaining

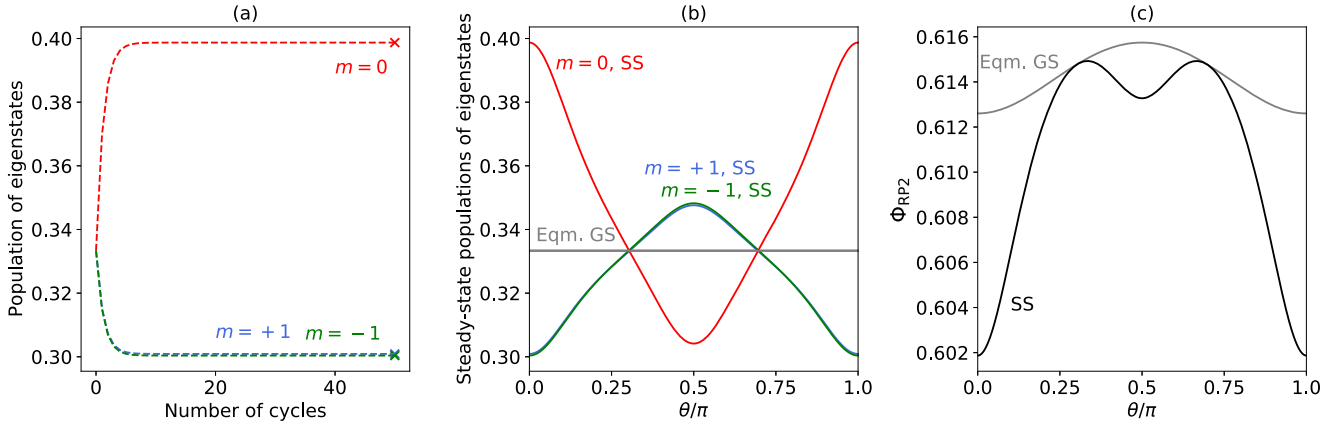

FIG. 3. Effect of retaining only S-branch nuclear polarization on the model symmetrized N5 radical pair. (a) Populations of the nuclear spin $\hat{I}_z$-eigenstates with quantum numbers $m = +1$, $m = 0$, and $m = -1$ for $\theta = 0$. The buildup with the number of cycles (dashed lines) together with the steady state populations (crosses). (b) Variation of the steady state (SS) populations with θ. (c) Dependence of Φ_{RP2} on θ in the steady state (black) and for a single cycle starting with equal initial populations of the three nuclear spin states (gray).

nuclear polarization lowers the minimum value of Φ_{RP2}, thereby increasing the anisotropy, $\Delta\Phi_{RP2}$.

This is precisely the effect that we are interested in, and we now present the changes in $\Delta\Phi_{RP2}$ for spin systems that are more closely related to the radical pair in cryptochrome.

D. Effect of polarization retention on $\Delta\Phi_{RP2}$

$\Delta\Phi_{RP2}$ [Eq. (20)] was calculated for each spin system using 3200 field directions ($0 \le \theta < \pi$ and $0 \le \phi < 2\pi$ in steps of $\pi/40$). Four dipolar tensors were considered: (a) no coupling, (b) the EPR value of $D = -11.2$ MHz with the dipolar axis parallel to the FAD plane normal (also used in Fig. 3), (c) the *Cl*Cry4 dipolar tensor [also used in Fig. 2(b)], and (d) the *Er*Cry4a MD dipolar tensor. In (a) and (b), the FAD and TrpH rings were in the same plane. In (c) and (d), the relative orientations in the *Cl*Cry4 and *Er*Cry4a MD configurations were adopted, respectively. Exchange interactions, known to be small from EPR measurements,[21] were not included here (but are discussed below). $\Delta\Phi_{RP2}$ was determined with (i) no, (ii) S-branch only, and (iii) full retention of nuclear polarization for five sets of nuclei: {N5, N5 + N10, N5 + NE1, N5 + N10 + NE1, and N5 + N10 + NE1 + HE1}. Figures 4(a)–4(d) show the calculated values of $\Delta\Phi_{RP2}$, while Figs. 4(e)–4(h) show the corresponding fractional changes in $\Delta\Phi_{RP2}$ resulting from the retention of nuclear polarization.

In the absence of electron–electron coupling [Fig. 4(a)], the effect of nuclear polarization on the reaction yield anisotropy is limited. This is not surprising given that the TSM mechanism is inoperative and the accumulation of polarization is therefore inefficient. Greater enhancements are found when dipolar interactions are included [Figs. 4(b)–4(d)]. However, it is noteworthy that the matching condition for TSM for a geomagnetic field of 50 μT ($\equiv$ 1.4 MHz) corresponds to a dipolar coupling parameter of $|D| \approx 4.2$ MHz, and all the dipolar couplings considered here [$D = -11.2$ MHz, -14.3 MHz, and -13.0 MHz for Figs. 4(b)–4(d), respectively] are too big for optimum TSM polarization. The larger enhancements seen for these dipolar couplings are limited to the smaller spin systems or when nuclear polarization is retained in both branches. While up to 40-fold increases in $\Delta\Phi_{RP2}$ are found for full retention of polarization in the N5 + N10 and N5 + N10 + NE1 systems in Fig. 4(b), the effect is much smaller for the more realistic scenario in which polarization is only preserved in the S-branch. Moreover, these enhancements do not carry across to the *Cl*Cry4 and *Er*Cry4a configurations [Figs. 4(c) and 4(d)] in which the flavin hyperfine and dipolar axes are no longer parallel. The differences in the results for these two configurations are attributed to small differences in the positions and orientations of the two radicals (see Tables S2 and S3 and Fig. S6 of the supplementary material).

Of the five sets of nuclear spins shown in Fig. 4, the three- and four-nuclei systems in the *Cl*Cry4 and *Er*Cry4a configurations are the most similar to the radical pair in cryptochrome. We find very little enhancement of the anisotropy in these cases. For the N5 + N10 + NE1 model system, with polarization retained only in the S-branch, there is, in fact, a small reduction in $\Delta\Phi_{RP2}$. The largest spin system studied (3N + HE1) predicts modest enhancements of 50%–100% when only the S-branch polarization is retained. The nuclei modeled here (N5, N10, NE1, and HE1) were chosen for their large anisotropic hyperfine interactions. We expect that inclusion of additional nuclei, with smaller anisotropy and differently oriented hyperfine tensors, would further diminish the enhancement in $\Delta\Phi_{RP2}$.

E. Dependence on k_S and k_F

Given that both the DD and DR nuclear polarization mechanisms depend on the degree of asymmetry in the decay rates of the singlet and triplet radical pairs, we considered additional values of the rate constants k_S and k_F. We calculated $\Delta\Phi_{RP2}$ for k_F/k_S ratios between 0.1 and 5 keeping $k_S = 10^6$ s^{-1}, using the same set of geomagnetic field directions as for Fig. 4. N5 + N10 and N5 + NE1 spin systems were simulated using the *Cl*Cry4 configuration of the

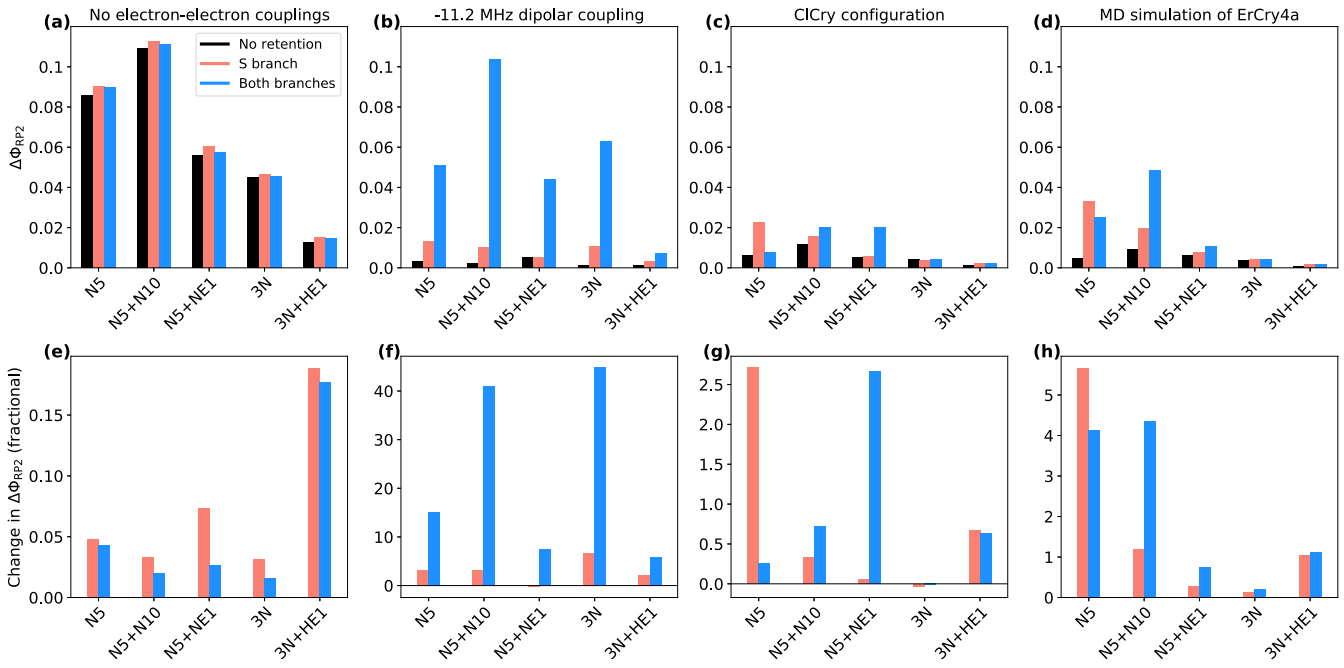

FIG. 4. $\Delta\Phi_{RP2}$, the anisotropy of the quantum yield of the formation of the signaling state [Eq. (20)], for a range of spin systems and three different dipolar tensors. The top row [(a)–(d)] shows $\Delta\Phi_{RP2}$; the bottom row [(e)–(h)] shows the fractional change, $\left(\Delta\Phi_{RP2} - \Delta\Phi^{nr}_{RP2}\right)/\Delta\Phi^{nr}_{RP2}$. Black: no retention. Red: S-branch retention. Blue: S- and F-branch retention.

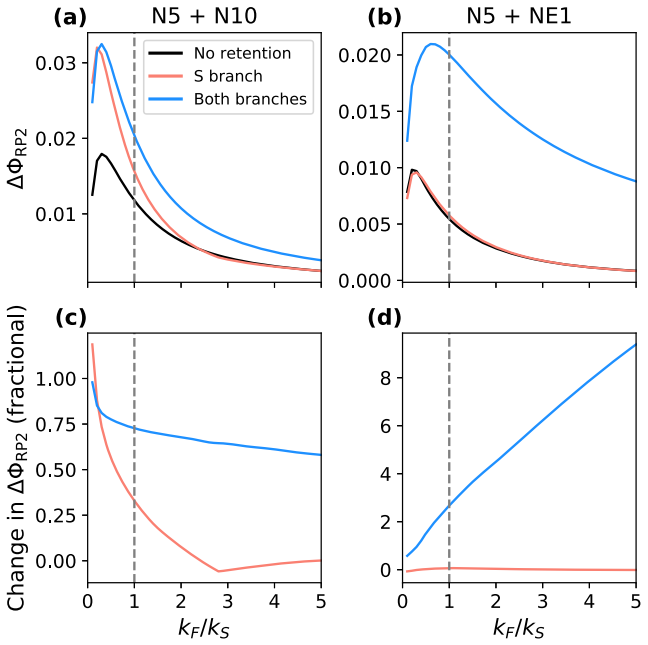

FIG. 5. $\Delta\Phi_{RP2}$ values [(a) and (b)] and their fractional changes [(c) and (d)] for the spin systems N5 + N10 and N5 + NE1 for $k_S = 10^6\ s^{-1}$ and k_F/k_S in the range 0.1–5. $k_F = k_S$ is shown as a gray dashed line.

radicals. The results are presented in Fig. 5. Similar calculations for k_S values other than $10^6\ s^{-1}$ are discussed in Sec. S4 of the supplementary material.

Maxima in both $\Delta\Phi_{RP2}$ and the absolute enhancement (i.e., $\Delta\Phi_{RP2} - \Delta\Phi^{nr}_{RP2}$) occur for $k_F/k_S \approx 1/3$. Retention of nuclear polarization shifts the position of the maximum: this is most clearly seen for the full-retention scenario for N5 + NE1, where the maximum for $\Delta\Phi_{RP2}$, and consequently, the absolute enhancement, is shifted to a higher value of k_F/k_S.

As shown in Fig. 4 (where $k_F/k_S = 1$), the increase in $\Delta\Phi_{RP2}$ when nuclear polarization is allowed to accumulate is larger when both branches are involved and depends on which nuclei are included. The enhancements in $\Delta\Phi_{RP2}$ for S-branch retention do not depend strongly on k_F/k_S.

F. Influence of exchange interactions

In addition to the results presented above, we also considered the effects of a small exchange interaction between the two electrons. Figure 6 shows the results of including the exchange coupling term in the radical pair Hamiltonians for J ranging from −5 MHz to +5 MHz (again using the *Cl*Cry4 configuration). Note that J is experimentally measured by EPR to be small,[21] and therefore, it is the values of J in the central region of the plots in Fig. 6 that most likely represent J in the radical pair *in vivo*. Calculations of $\Delta\Phi_{RP2}$ were performed using the same combinations of nuclei and field directions as for Fig. 5.

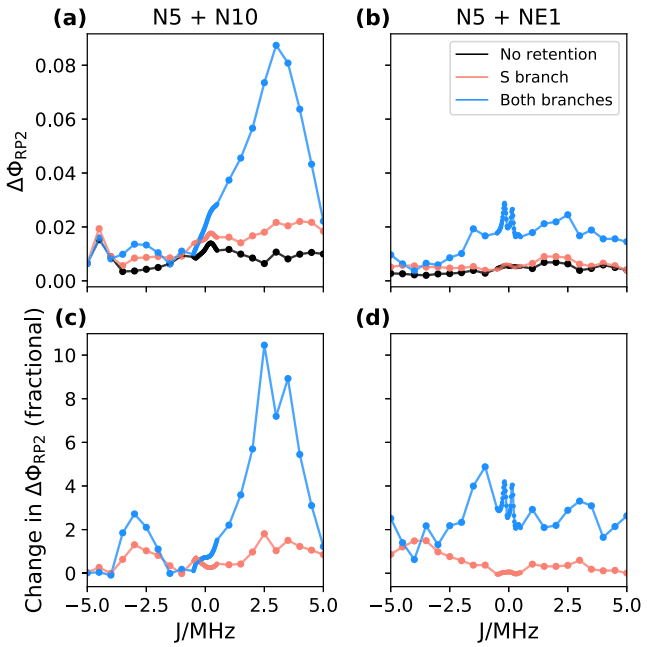

FIG. 6. $\Delta\Phi_{RP2}$ values [(a) and (b)] and their fractional changes [(c) and (d)] for the spin systems N5 + N10 and N5 + NE1 for a range of J values between −5 MHz and +5 MHz. $\Delta\Phi_{RP2}$ was calculated with 0.02 MHz steps in the range −0.5 MHz < J < +0.5 MHz and 0.5 MHz steps otherwise.

As for the $J = 0$ case, large enhancements are mainly only observed for full polarization retention. The overall behavior and magnitudes of absolute and fractional enhancements do not deviate far from $J = 0$ except for large positive J in the N5 + N10 case.

IV. CONCLUDING REMARKS

We have used spin dynamics simulations of models of [$FAD^{\bullet-}$ $Trp_CH^{\bullet+}$] radical pairs in cryptochrome to assess whether accumulation of nuclear polarization in multiple photocycles around the reaction scheme shown in Fig. 1 could lead to significant enhancements in the sensitivity with which the protein responds to the direction of the geomagnetic field. Figures 2 and 3 provide a proof of concept by showing that the yield of RP2, from which the signaling state of the protein is formed, depends on the initial nuclear spin state of the radical pair, that nuclear spin polarization can accumulate in sequential photochemical cycles, and that a direct consequence is a change in the anisotropy of the yield of RP2 ($\Delta\Phi_{RP2}$), the quantity that determines the compass sensitivity.

Simulations of simple models of the [$FAD^{\bullet-}$ $TrpH^{\bullet+}$] state of cryptochrome (Fig. 4) show that significant enhancements in $\Delta\Phi_{RP2}$ are restricted to (a) the simpler model spin systems, (b) the case where nuclear polarization is retained in both reaction branches (Fig. 1), and (c) an idealized configuration of the radicals in which their aromatic rings are stacked one above the other. All the three conditions suggest that the enhancements in $\Delta\Phi_{RP2}$ will be smaller in reality, at least within the scope of the models considered. (a) It is the larger spin systems, in particular, N5 + N10 + NE1 + HE1, that more closely resemble the radical pair in cryptochrome. (b) Full retention of polarization in both branches is much less likely to occur *in vivo* than in the S-branch alone. (c) The radicals in cryptochrome do not have the idealized relative orientations that seem to optimize the enhancement in $\Delta\Phi_{RP2}$. Variation of the rate constants for the reactions of RP1 (Fig. 5) and inclusion of plausible exchange interactions (Fig. 6) do not lead to significantly larger values of $\Delta\Phi_{RP2}$ under conditions likely to pertain *in vivo*.

We therefore conclude that accumulation of nuclear polarization seems unlikely to be the source of significant improvements in the performance of cryptochrome-based radical pair magnetoreceptors, at least in the form realized here.

SUPPLEMENTARY MATERIAL

See the supplementary material for details of the spin dynamics and molecular dynamics simulations, Kramers theorem, additional $\Delta\Phi_{RP2}$ calculations, and calculated hyperfine tensors.

ACKNOWLEDGMENTS

We grateful acknowledge the financial support of the Deutsche Forschungsgemeinschaft (Project Nos. 395940726—SFB 1372 *Magnetoreception and Navigation in Vertebrates* and GRK1885) and the European Research Council (under the European Union's Horizon 2020 research and innovation programme, Grant Agreement No. 810002, Synergy Grant, *QuantumBirds*). D.R.K. is grateful for support provided by the Defense Science and Technology Laboratory (Dstl; Contract No. DSTLX-1000139168). I.A.S. thanks the Lundbeck Foundation and the Volkswagen Foundation (Lichtenberg Professorship to I.A.S.). Computational resources for the simulations were provided by the DeiC National HPC Center, SDU, and the CARL Cluster at the Carl-von-Ossietzky University of Oldenburg, which is supported by the DFG under INST Grant No. 184/157-1 FUGG and the Ministry of Science and Culture (MWK) of the Lower Saxony State. We thank Ilya Kuprov for calculations of hyperfine coupling parameters, Lachlan Lindoy and Jiate Luo for helpful discussions of the Kramers theorem, and Henrik Mouritsen for helpful comments on this manuscript.

DATA AVAILABILITY

Data sharing is not applicable to this article as no new data were created or analyzed in this study.

REFERENCES

[1] W. Wiltschko, Z. Tierpsychol. **25**, 537 (1968).
[2] W. Wiltschko and R. Wiltschko, Science **176**, 62 (1972).
[3] R. Wiltschko and W. Wiltschko, *Magnetic Orientation in Animals* (Springer-Verlag, Berlin, 1995).
[4] H. Mouritsen, *Sturkie's Avian Physiology*, edited by C. Scanes (Elsevier, New York, 2014), pp. 113–133.
[5] H. Mouritsen, Nature **558**, 50 (2018).
[6] C. M. Hein, M. Zapka, D. Heyers, S. Kutzschbauch, N.-L. Schneider, and H. Mouritsen, J. R. Soc. Interface **7**, S227 (2010).

[7]C. M. Hein, S. Engels, D. Kishkinev, and H. Mouritsen, Nature **471**, E1 (2011).
[8]S. Engels, C. M. Hein, N. Lefeldt, H. Prior, and H. Mouritsen, PLoS One **7**, e43271 (2012).
[9]M. Zapka, D. Heyers, C. M. Hein, S. Engels, N.-L. Schneider, J. Hans, S. Weiler, D. Dreyer, D. Kishkinev, J. M. Wild, and H. Mouritsen, Nature **461**, 1274 (2009).
[10]H. Mouritsen, D. Heyers, and O. Güntürkün, Annu. Rev. Physiol. **78**, 133 (2016).
[11]K. Schulten, C. E. Swenberg, and A. Weller, Z. Phys. Chem. **111**, 1 (1978).
[12]T. Ritz, S. Adem, and K. Schulten, Biophys. J. **78**, 707 (2000).
[13]P. J. Hore and H. Mouritsen, Annu. Rev. Biophys. **45**, 299 (2016).
[14]I. A. Solov'yov, D. E. Chandler, and K. Schulten, Biophys. J. **92**, 2711 (2007).
[15]M. Liedvogel, K. Maeda, K. Henbest, E. Schleicher, T. Simon, C. R. Timmel, P. J. Hore, and H. Mouritsen, PLoS One **2**, e1106 (2007).
[16]K. Maeda, A. J. Robinson, K. B. Henbest, H. J. Hogben, T. Biskup, M. Ahmad, E. Schleicher, S. Weber, C. R. Timmel, and P. J. Hore, Proc. Natl. Acad. Sci. U. S. A. **109**, 4774 (2012).
[17]C. Nießner, S. Denzau, J. C. Gross, L. Peichl, H.-J. Bischof, G. Fleissner, W. Wiltschko, and R. Wiltschko, PLoS One **6**, e20091 (2011).
[18]P. Bolte, F. Bleibaum, A. Einwich, A. Günther, M. Liedvogel, D. Heyers, A. Depping, L. Wöhlbrand, R. Rabus, U. Janssen-Bienhold, and H. Mouritsen, PLoS One **11**, e0147819 (2016).
[19]C. Nießner, J. C. Gross, S. Denzau, L. Peichl, G. Fleissner, W. Wiltschko, and R. Wiltschko, PLoS One **11**, e0150377 (2016).
[20]A. Günther, A. Einwich, E. Sjulstok, R. Feederle, P. Bolte, K.-W. Koch, I. A. Solov'yov, and H. Mouritsen, Curr. Biol. **28**, 211 (2018).
[21]T. Hochstoeger, T. Al Said, D. Maestre, F. Walter, A. Vilceanu, M. Pedron, T. D. Cushion, W. Snider, S. Nimpf, G. C. Nordmann, L. Landler, N. Edelman, L. Kruppa, G. Dürnberger, K. Mechtler, S. Schuechner, E. Ogris, E. P. Malkemper, S. Weber, E. Schleicher, and D. A. Keays, Sci. Adv. **6**, eabb9110 (2020).
[22]D. R. Kattnig, E. W. Evans, V. Déjean, C. A. Dodson, M. I. Wallace, S. R. Mackenzie, C. R. Timmel, and P. J. Hore, Nat. Chem. **8**, 384 (2016).
[23]D. M. W. Sheppard, J. Li, K. B. Henbest, S. R. T. Neil, K. Maeda, J. Storey, E. Schleicher, T. Biskup, R. Rodriguez, S. Weber, P. J. Hore, C. R. Timmel, and S. R. MacKenzie, Sci. Rep. **7**, 42228 (2017).
[24]R. Kaptein and J. L. Oosterhoff, Chem. Phys. Lett. **4**, 195 (1969).
[25]G. L. Closs, J. Am. Chem. Soc. **91**, 4552 (1969).
[26]W. Wiltschko and R. Wiltschko, J. Exp. Biol. **204**, 3295 (2001).
[27]R. Wiltschko, K. Stapput, P. Thalau, and W. Wiltschko, J. R. Soc. Interface **7**, S163 (2010).
[28]T. Ritz, P. Thalau, J. B. Phillips, R. Wiltschko, and W. Wiltschko, Nature **429**, 177 (2004).
[29]T. Ritz, R. Wiltschko, P. J. Hore, C. T. Rodgers, K. Stapput, P. Thalau, C. R. Timmel, and W. Wiltschko, Biophys. J. **96**, 3451 (2009).
[30]H. G. Hiscock, H. Mouritsen, D. E. Manolopoulos, and P. J. Hore, Biophys. J. **113**, 1475 (2017).
[31]D. R. Kattnig, I. A. Solov'yov, and P. J. Hore, Phys. Chem. Chem. Phys. **18**, 12443 (2016).
[32]D. R. Kattnig, J. K. Sowa, I. A. Solov'yov, and P. J. Hore, New J. Phys. **18**, 063007 (2016).
[33]D. Kobylkov, J. Wynn, M. Winklhofer, R. Chetverikova, J. Xu, H. Hiscock, P. J. Hore, and H. Mouritsen, J. R. Soc. Interface **16**, 20190716 (2019).
[34]S. Engels, N.-L. Schneider, N. Lefeldt, C. M. Hein, M. Zapka, A. Michalik, D. Elbers, A. Kittel, P. J. Hore, and H. Mouritsen, Nature **509**, 353 (2014).
[35]S. Schwarze, N.-L. Schneider, T. Reichl, D. Dreyer, N. Lefeldt, S. Engels, N. Baker, P. J. Hore, and H. Mouritsen, Front. Behav. Neurosci. **10**, 55 (2016).
[36]R. Kaptein, *Biological Magnetic Resonance*, edited by L. J. Berliner and J. Reuben (Plenum Press, New York, 1982), Vol. 4, pp. 145–191.
[37]P. J. Hore and R. W. Broadhurst, Prog. Nucl. Magn. Reson. Spectrosc. **25**, 345 (1993).
[38]G. Richter, S. Weber, W. Römisch, A. Bacher, M. Fischer, and W. Eisenreich, J. Am. Chem. Soc. **127**, 17245 (2005).
[39]W. Eisenreich, M. Joshi, S. Weber, A. Bacher, and M. Fischer, J. Am. Chem. Soc. **130**, 13544 (2008).
[40]S. S. Thamarath, J. Heberle, P. J. Hore, T. Kottke, and J. Matysik, J. Am. Chem. Soc. **132**, 15542 (2010).
[41]H. Wu, A. Scholten, A. Einwich, H. Mouritsen, and K.-W. Koch, Sci. Rep. **10**, 7364 (2020).
[42]M. H. Levitt, Annu. Rev. Phys. Chem. **63**, 89 (2012).
[43]G. Pileio, Prog. Nucl. Magn. Reson. Spectrosc. **56**, 217 (2010).
[44]J. Matysik, A. Diller, E. Roy, and A. Alia, Photosynth. Res. **102**, 427 (2009).
[45]B. E. Bode, S. S. Thamarath, K. B. S. S. Gupta, A. Alia, G. Jeschke, and J. Matysik, *Hyperpolarization Methods NMR Spectroscopy*, edited by L. T. Kuhn (Springer Berlin Heidelberg, Berlin, Heidelberg, 2013), pp. 105–121.
[46]R. A. Goldstein and S. G. Boxer, Biophys. J. **51**, 937 (1987).
[47]A. McDermott, M. G. Zysmilich, and T. Polenova, Solid State Nucl. Magn. Reson. **11**, 21 (1998).
[48]T. Polenova and A. E. McDermott, J. Phys. Chem. B **103**, 535 (1999).
[49]G. Jeschke, J. Chem. Phys. **106**, 10072 (1997).
[50]G. Jeschke, J. Am. Chem. Soc. **120**, 4425 (1998).
[51]G. Jeschke, B. C. Anger, B. E. Bode, and J. Matysik, J. Phys. Chem. A **115**, 9919 (2011).
[52]P. Müller, J. Yamamoto, R. Martin, S. Iwai, and K. Brettel, Chem. Commun. **51**, 15502 (2015).
[53]F. Cailliez, P. Müller, T. Firmino, P. Pernot, and A. De La Lande, J. Am. Chem. Soc. **138**, 1904 (2016).
[54]N. S. Babcock and D. R. Kattnig, J. Phys. Chem. Lett. **11**, 2414 (2020).
[55]R. Haberkorn, Mol. Phys. **32**, 1491 (1976).
[56]S. Worster, H. Mouritsen, and P. J. Hore, J. R. Soc. Interface **14**, 20170405 (2017).
[57]H. G. Hiscock, T. W. Hiscock, D. R. Kattnig, T. Scrivener, A. M. Lewis, D. E. Manolopoulos, and P. J. Hore, Q. Rev. Biophys. **52**, e9 (2019).
[58]A. A. Lee, J. C. S. Lau, H. J. Hogben, T. Biskup, D. R. Kattnig, and P. J. Hore, J. R. Soc. Interface **11**, 20131063 (2014).
[59]B. D. Zoltowski, Y. Chelliah, A. Wickramaratne, L. Jarocha, N. Karki, W. Xu, H. Mouritsen, P. J. Hore, R. E. Hibbs, C. B. Green, and J. S. Takahashi, Proc. Natl. Acad. Sci. U. S. A. **116**, 19449 (2019).
[60]C. R. Timmel, S. Richert, S. Weber, T. L. Pitcher, and G. Moise, unpublished results (2020).
[61]H. Kramers, Proc. K. Akad. Wet. **33**, 959 (1930).
[62]M. J. Klein, Am. J. Phys. **20**, 65 (1952).
[63]C. R. Timmel, U. Till, B. Brocklehurst, K. A. McLauchlan, and P. J. Hore, Mol. Phys. **95**, 71 (1998).
[64]A. M. Lewis, T. P. Fay, D. E. Manolopoulos, C. Kerpal, S. Richert, and C. R. Timmel, J. Chem. Phys. **149**, 034103 (2018).